Anal Bioanal Chem (2011) 401:795–801
DOI 10.1007/s00216-011-5069-1

PAPER IN FOREFRONT

Functional histology of glioma vasculature by FTIR imaging

Razia Noreen · Raphael Pineau · Chia-Chi Chien · Mariangela Cestelli-Guidi · Yeukuang Hwu · Augusto Marcelli · Michel Moenner · Cyril Petibois

Received: 6 January 2011 / Revised: 8 March 2011 / Accepted: 27 April 2011 / Published online: 10 May 2011

Abstract Fourier-transform infrared (FTIR) imaging has been used to investigate brain tumor angiogenesis using a mice solid tumor model and bare-gold (∅ 25 nm) or $BaSO_4$ (∅ 500 nm) nanoparticles (NP) injected into blood vasculature. FTIR images of 20-μm-thick tissue sections were used for chemical histology of healthy and tumor areas. Distribution of $BaSO_4$-NP (using the 1,218–1,159 cm^{-1} spectral interval) revealed clearly all details of blood vasculature with morphological abnormalities of tumor capillaries, while Au-NP (using the 1,046–1,002 cm^{-1} spectral interval) revealed also diffusion properties of leaky blood vessels. Diffusion of Au-NP out of vascular space reached 64±29 μm, showing the fenestration of "leaky" tumor blood vessels, which should allow small NP (<100 nm, as for Au-NP) to diffuse almost freely, while large NP should not (as for $BaSO_4$-NP in this study). Therefore, we propose to develop FTIR imaging as a convenient tool for functional molecular histology imaging of brain tumor vasculature, both for identifying blood capillaries and for determining the extravascular diffusion space offered by vessel fenestration.

Keywords Bioanalytical methods · IR spectroscopy/Raman spectroscopy · Nanoparticles/Nanotechnology · Spectroscopy/Instrumentation

Published in the special issue *Imaging Techniques with Synchrotron Radiation* with Guest Editor Cyril Petibois.

R. Noreen · C. Petibois (✉)
Université de Bordeaux,
CNRS UMR 5248 CBMN, 2 Rue Robert Escarpit,
33604 Pessac, France
e-mail: c.petibois@cbmn.u-bordeaux.fr

R. Pineau · M. Moenner
INSERM U920, Université de Bordeaux 1,
Avenue des facultés,
33604 Pessac, France

C.-C. Chien · Y. Hwu
Institute of Physics, Academia Sinica,
Nankang,
Taipei 115 Taiwan, China

M. Cestelli-Guidi · A. Marcelli
INFN LNF,
40 Via Enrico Fermi,
00044 Frascati-Roma, Italy

Introduction

Glioblastomas are a class of primary brain tumors characterized by mixed solid and diffuse volumes, both of which have different effects on angiogenesis. Basically, the solid tumor parts induce neovascularization with the sprouting of numerous capillaries at the periphery of tumor mass, while diffuse tumor parts induce primarily cooption of existing vascular network for further ramification of tumor mass. One common aspect of these angiogenic processes is that blood capillaries become leaky [1], thus breaking the blood–brain barrier (BBB) for diffusion of plasma molecular contents out of the vascular space [2, 3]. The consequence is that the extravascular diffusion space defined by leaky blood vessels is the area where tumor cells find the best micro-environment for growth and division [4]. Considering fenestraes from the functional point of view, permeability to molecules is independent of pore cutoff size as long as the diameter of the molecule is much less than the pore diameter [5], probably 1/3 to 1/5. Therefore, defining a therapeutic strategy against tumor cells requires imaging tumor vasculature as well as its fenestraes and the extravascular diffusion space they

provide. However, such in vivo functional imaging is not yet available. It should combine both high-resolution capability (tumor microvessels are a few micrometers in diameter, and the fenestraes are 20–60 nm in diameter [2], randomly distributed over capillary length, i.e., along a 100–500 μm distance [6]), and with chemical information rendering. Current in vivo imaging techniques (MRI and PET) remain unable to reveal pathological objects, such as metastases or tumors with diameter <5–10 mm. This is due to the spatial resolution offered by these techniques, which cannot go below 1-mm at the best for human applications, 100-μm in small animals [7–9]. It is thus necessary to use alternative imaging techniques for ex vivo histology examination [10], where the biodistribution of defined chemical species is required. However, except electron microscopy, no technique has been able to provide significant information about vascular endothelial cells fenestration under tumorogenic stress in glioma development [6]. It was able to show fenestraes on blood capillary vascular membrane. Immunohistochemistry can be used also for determining the extravascular diffusion of plasma molecular moieties using Hoechst-33342 fluorescent probe [11]. However, combination of these techniques is not possible due to exclusive sample preparations and handling protocols.

Fourier-transform infrared (FTIR) imaging has been proposed as a chemical probe of biosample molecular contents, notably to investigate pathological disorders, such as cancer [12]. The technique is based upon the absorption of IR radiation by covalent bonds of the molecules in presence, thus revealing almost all organic contents of a sample [10]. The technique is widely used for analyzing ratios between families of molecules in biosamples, cells, or tissues, notably for the proteins, lipids, and saccharides [13]. Inorganic compounds may be also analyzed, notably those containing chemical derivatives from sulfur, selenium, bromine, iodine, vanadium, chromium, chlorine, phosphate, and manganese [14]. These inorganic species have usually very intense and characteristic bands below 1,400 cm^{-1}, which spectral interval is also out of the main IR absorptions found on most concentrated compounds of biosamples, namely the proteins (1,700–1,500 cm^{-1} for amides I and II). Inorganic nanoparticles are now widely used as imaging agents, notably those based on gadolinium and barium for MRI, radioactive fluorine for PET, etc. Here, we propose the use of FTIR imaging as a functional histology tool for analyzing both the molecular contents of brain tissues as well as inorganic NP used as contrast agent highlighting angiogenic properties of solid and diffuse tumors. We used immunodeficient mice which were implanted intracranially with tumor cells for glioma development over 25 days before to inject $BaSO_4$ or bare-gold (Au) nanoparticles (NP) for revealing brain blood vasculature. FTIR imaging was further used for studying blood vasculature of solid and diffuse models of glioma tumors. To test the efficiency of the approach, $BaSO_4$ was chosen as highly absorption IR model of NP [15], while Au was used as a low absorption IR model of NP [16].

Methods

Samples Three experimental conditions were tested for FTIR imaging of brain tumor tissues: A—mice perfused with phosphate buffer saline (PBS) before $BaSO_4$ (∅ 500 nm) or bare-gold NP (Au-NP, ∅ 25 nm) injection, B—mice perfused with paraformaldehyde (PFA) before $BaSO_4$ or bare-gold NP injection, and C—mice perfused with PFA before $BaSO_4$ or bare-gold NP injection and for which brains were further stained with sucrose. Thirty rag-gamma mice were used for this study, equally divided in three groups of 10 for A, B, and C conditions. U87-Ctrl (solid tumor model) and U87-DN (diffuse tumor model) glioma tumor cells were cultured in petri dish before implantation in brain. Cells (3.10^6) were implanted in mice brain at Bregma −0.1, 2.2 mm lateral, and 3.0 mm in depth. Tumor growth lasted 10 to 25 days for obtaining different sample sizes. Vasculature filling with $BaSO_4$ or Au-NP occurred after PBS or PFA perfusion to remove blood. PBS and PFA perfusions were performed at carotid before NP perfusion to ensure the filling of brain hemisphere where tumors have grown. Therefore, ten experimental conditions could be analyzed: 1 and 2=healthy tissue (contralateral hemisphere of tumors, notated H-PBS and H-PFA), 3 and 4=solid tumor tissue with Au-NP (notated S-Au-PBS and S-Au-PFA), 5 and 6=solid tumor tissue with $BaSO_4$-NP (notated S-$BaSO_4$-PBS and S-$BaSO_4$-PFA), 7 and 8=diffuse tumor tissue with Au-NP (notated D-Au-PBS and D-Au-PFA), and 9 and 10=diffuse tumor tissue with $BaSO_4$-NP (notated D-$BaSO_4$-PBS and D-$BaSO_4$-PFA).

FTIR imaging For every tumor specimen, frozen tissue was deposited on cooled glue for cryostat (−20 °C, 3050-TM, Leica-Microsystems, France) to avoid tissue embedding. Serial frozen sections, 20 μm in thickness, were transferred on ZnSe windows for FTIR spectral imaging. All tissue sections were dried in air before further processing. Tumor sections, 20 μm in thickness, were used for FTIR analysis using Hyperion 3000 spectral imaging system equipped with a Vertex 70 spectrometer (Bruker-Optics, France) and with a liquid-N_2 cooled focal plane array (64×64 elements 40×40 microns each) detector and a Globar source. A ×15 magnification level and condenser were used for obtaining a final FTIR image with pixels dimension of 2.6×2.6 μm, thus at ~λ/2 for the mid-IR spectral interval. All visible images were obtained in transmission mode from the tumor

sections in the 4,000–900 cm^{-1} range by using 128 scans with spectral resolution of 8 cm^{-1}.

Spectral data treatment Integration method has been applied on all the tissue samples by using subroutine of Opus 6.5 software (Bruker-Optics, France). Five different spectral ranges have been selected for integration of these images. FTIR integration of images was performed with different spectral ranges: 1,216–1,158, 1,148–1,101, 1,101–1,038, 1,101–1,034, 992–969, and 1,148–969 cm^{-1} for $BaSO_4$-NP; and 1,700–1,600, 1,150–950, 1,150–950/1,700–1,600, 1,700–1,480, and 1,150–950/1,700–1,480 cm^{-1} for Au-NP. The integration methods have been used to find out the highest absorption contrast between blood vessels and tissue due to the presence of contrast agents. The capillary surface area has also been calculated for each blood vessel present in the tissue sections of solid and diffuse tumors. Results are presented as means±SD. Differences between series of data were determined using the Student *t* test. Confidence limit was set at 1% or 5% ($P<0.01$ or 0.05) as indicated in text, tables, and figures.

Results and discussions

With the help of contrast agents, $BaSO_4$ and Au-NP, FTIR imaging could provide high-resolution structural 3D information of blood vessels and offered a unique opportunity for imaging, quantification, and analysis of vascular network of the brain tumors. Several blood capillaries were selected on every tissue section for FTIR image acquisition. Averaged spectra ($n=50$) were extracted from the each blood capillary and tissue sections with 4,000–900 cm^{-1} spectral intervals (Fig. 1). Spectral integration method was applied on all tumor samples according to their selected spectral interval for Au- and $BaSO_4$-NP of each group. As shown in the Fig. 1, the capillary surface area has also been calculated from these images. The yellow red absorption regions depicting accumulation of NP in tumor blood vessels are clearly show in the figures. The diffusion properties of tumor vessels were analyzed by the FTIR imaging with characteristic absorption bands of NP.

Tumor models perfused with PBS With solid tumor models perfused with PBS (Tables 1 and 2), the results obtained by integration of absorption bands showed that the highest values obtained for blood capillaries and tissues using the 1,148–969 cm^{-1} spectral interval for $BaSO_4$-NP (10.7±2.5 vs. 33.3±6.7 squared a.u.; tissue vs. capillaries, respectively) and the 1,700–1,480 cm^{-1} spectral interval for Au-NP (54.2±6.5 vs. 78.6 ±12 squared a.u.; tissue vs. capillaries, respectively). However, the largest difference between integration values of blood capillaries and tissues were found using the 1,216–1,158 cm^{-1} spectral interval for $BaSO_4$-NP (0.0±0.0 vs. 2.6±1.7 squared a.u.; tissue vs. capillaries, respectively) and using 1,150–950 cm^{-1} spectral interval for Au-NP (7.3±0.9 vs. 11.2±2.9 squared a.u.; tissue vs. capillaries, respectively). The null values obtained on 1,216–1,158 cm^{-1} spectral interval on tissues traduce a characteristic absorption of $BaSO_4$-NP found at surface of spectrum curve, and the relatively good result obtained on Au-NP using the 1,150–950 cm^{-1} spectral interval reflects the small sharp band found on Au-NP spectrum at this spectral interval (Fig. 2).

With diffuse tumor models perfused with PBS (Tables 1 and 2), results were found globally comparable with those obtained on solid tumors. The spectral interval giving the best discrimination between tissue and capillaries using $BaSO_4$-NP was 1,148–969 cm^{-1}, if we consider absolute values (6.3±1.7 vs. 26.7±1.9 squared a.u.; tissue vs. capillaries, respectively), or 1,216–1,158 cm^{-1}, if we consider relative difference (0.0±0.0 vs. 3.1±1.1 squared a.u.; tissue vs. capillaries, respectively; Fig. 3). For Au-NP, results paralleled those obtained on solid tumors using the 1,150–950 cm^{-1} (6.6±1.3 vs. 10.3±1.3 squared a.u.; tissue vs. capillaries, respectively).

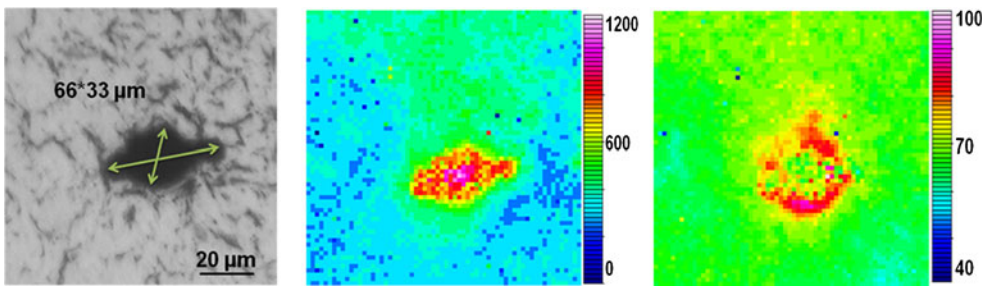

Fig. 1 FTIR imaging of diffuse tumor perfused with PBS and Au-NP. *Left*—mice brain tumor tissue section (20-µm thick) with a large coopted blood vessel. *Center*—2D-FTIR image of blood vessel (4,000–900 cm^{-1} spectral interval). *Right*—2D-FTIR image with highest absorption contrast for Au-NP vs. tissue using the 1,700–1,480 cm^{-1} spectral interval

Table 1 Spectral data treatment of FTIR images from tumors perfused with PBS and $BaSO_4$-NP

Spectral Interval (cm^{-1})	Solid tumors (PBS)		Diffuse tumors (PBS)		Healthy tissue
	Tissues	Capillaries	Tissues	Capillaries	Tissue
1,216–1,158	0.0±0.0[b]	2.6±1.7[b]	0.0±0.0[c]	3.1±1.1[c]	0.0±0.0
1,148–1,101	0.0±0.0[b]	1.7±1.0[b]	0.0±0.0[c]	1.3±0.7[c]	0.0±0.0
1,101–1,038	2.4±0.5[a,b]	6.1±2.8[b]	1.6±0.5[a,c]	5.0±1.5[c]	2.9±1.9
1,101–1,034	2.8±0.6[a,b]	7.4±2.8[b]	1.9±0.6[a,c]	6.1±1.4[c]	3.6±2.4
992–969	0.0±0.0[a,b]	0.4±0.1[b]	0.03±0.01[a,c,d]	0.4±0.1[c]	0.0±0.0[d]
1,148–969	10.7±2.5[a,b]	33.3±6.7[b]	6.3±1.7[a,c,d]	26.7±1.9[c]	15.4±9.6[d]

All values are mean±SE of spectral integration results obtained from different spectral intervals

[a] Tumor solid is significantly different from tumor diffuse

[b] Tumor solid is significantly different from capillaries solid

[c] Tumor diffuse is significantly different from capillaries diffuse

[d] Healthy tissue is significantly different from diffuse tumor. No significant difference was found between capillaries solid and diffuse. n=6 samples and 50 spectra per sample

Tumor models perfused with PFA PFA staining is known to change organic compounds chemistry, such as protein unfolding [17]. It is widely used for histology when the study of tissue must render the morphology and given molecular information, which is obtained by labeling. However, using a vibrational spectroscopy technique such as FTIR imaging, the staining of a tissue with PFA can modify strongly the results. Our study (Table 3) shows clearly that utilization of the same spectral intervals as for tissue models perfused with PBS could not give comparable results. We found aberrant results using the 1,216–1,158 cm^{-1} spectral interval for $BaSO_4$-NP for the solid tumor model (0.0±0.0 vs. 1.9±0.5 squared a.u.; tissue vs. capillaries, respectively) as well as for the diffuse tumor model (0.0±0.0 vs. 0.0±0.0 squared a.u.; tissue vs. capillaries, respectively). No major difference was found with healthy tissues, thus invalidating the use of this spectral interval for molecular histology of tumors. Results obtained on solid and diffuse tumors stained with PFA and using Au-NP as contrast agents of blood vasculature could not reveal systematic discrimination between tissues and capillaries using the spectral intervals shown in Table 2 (data not shown).

Extravascular diffusion space probed by NP The second aim of this study was to test the potential of selected contrast agents for determining the extravascular diffusion space of leaky blood vessels in solid and diffuse models of glioma implanted and developed in mice brain. One should first consider that only tumor models perfused with PBS

Table 2 Spectral data treatment of FTIR images from tumors perfused with PBS and Au-NP

Spectral Interval (cm^{-1})	Solid tumors (PBS)		Diffuse tumors (PBS)		Healthy tissue
	Tissues	Capillaries	Tissues	Capillaries	Tissue
1,150–950=A	7.3±0.9[b]	11.2±2.9[b]	6.6±1.3[cd]	10.3±1.3[c]	12.8±2.8[d]
1,700–1,600=B	28.0±3.6[b]	40.0±6.0[b]	28.7±5.0	35.5±6.0	26.2±4.6
1,700–1,480=C	54.2±6.5[b]	78.6±12.0[b]	55.7±7.0[c]	68.0±11.6[c]	51.9±9.8
A/B	0.26±0.03[a,e]	0.28±0.05	0.23±0.01[a,c,d]	0.29±0.04[c]	0.5±0.07[d,e]
A/C	0.14±0.01[a,e]	0.15±0.09	0.12±0.01[a,c,d]	0.15±0.09[c]	0.25±0.04[d,e]

All values are mean±SE of spectral integration results obtained from different spectral intervals

[a] Tumor solid is significantly different from tumor diffuse

[b] Tumor solid is significantly different from capillaries solid

[c] Tumor diffuse is significantly different from capillaries diffuse

[d] Healthy tissue is significantly different from diffuse tumor

[e] Healthy tissue is significantly different from solid tumor. n=6 samples and 50 spectra per sample

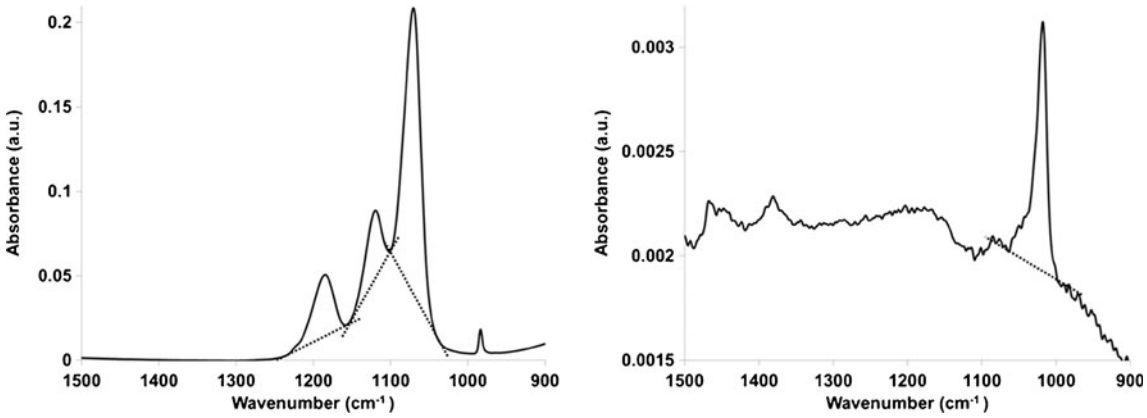

Fig. 2 $BaSO_4$ and Au-NP FTIR spectra with corresponding spectral intervals used for FTIR image reconstruction

could be used for studying extravascular diffusion. It is also important to take into account the size of NP ($BaSO_4$-NP ∅=500 nm and Au-NP ∅=25 nm), which obviously affected the potential of extravascular diffusion (Fig. 3). Using the different tissue sections of this study, it was found that only a few blood capillaries exhibited extravascular diffusion of NP (21/121 for Au-NP=18%; 9/106 for $BaSO_4$-NP=8%). Considering the tumor models we used, the 21 capillaries found to exhibit extravascular diffusion of Au-NP were distributed as follows: 14 for solid tumor vasculature and seven for diffuse tumor vasculature; interestingly, this distribution was three for solid tumor vasculature and six for diffuse tumor vasculature while using $BaSO_4$-NP. Thus, our result using small Au-NP showed that more fenestraes existed in solid tumor model and the use of large $BASO_4$-NP showed that larger fenestraes could be found in diffuse tumor model (Fig. 4). It was also noteworthy that no blood capillary (n=97) belonging to healthy brain tissues exhibited extravascular diffusion of both Au and $BaSO_4$ NP, thus confirming that only leaky tumor blood vessels allowed diffusing NP out of the blood brain barrier.

Discussion

Conventional imaging techniques are not sensitive to detect the early stages of tumor grow associated to its vasculature development, but imaging with NP contrast agents can facilitate the examination of tissues to reveal peculiar aspects of their organization. Here, gold and barium-sulfate nanoparticles have been used for determining the potential of FTIR imaging to reveal both the presence of blood capillaries in tissues (healthy and tumor models) and their extravascular diffusion properties, more particularly, the distance of diffusion out of the BBB. The choice of two NP with two different sizes was to test both the ability of FTIR imaging to identify low- and high-absorbing specimens (Au vs. $BaSO_4$, respectively) as well as to test the potential of the NP to discriminate the properties (size and distribution) of fenestraes in solid and diffuse models of glioma tumors. We succeeded in demonstrating that both low and high IR absorbing contrast agents could be used for imaging blood capillaries in tissue sections. Au-NP could be clearly identified in capillaries lumen using non-specific IR absorption bands, the 1,700–1,480 cm^{-1} interval

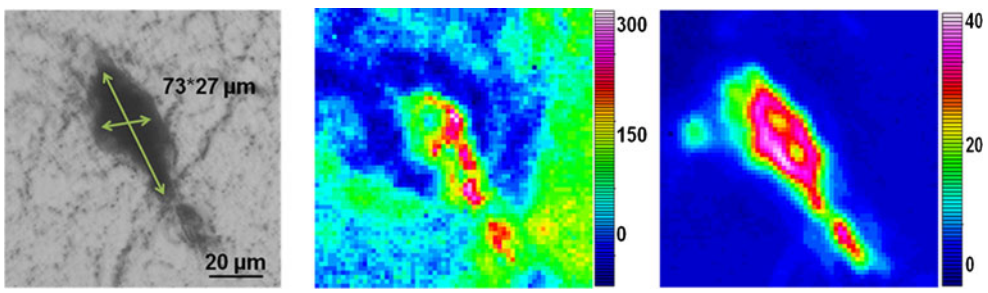

Fig. 3 FTIR imaging of diffuse tumor perfused with PBS and $BaSO_4$-NP. *Left*—mice brain tumor tissue section (20-µm thick) with a large coopted blood vessel. *Center*—2D-FTIR image of blood vessel (4,000–900 cm^{-1} spectral interval). *Right*—2D-FTIR image with highest absorption contrast for $BaSO_4$-NP vs. tissue using the 1,148–969 cm^{-1} spectral interval

Table 3 Spectral data treatment of FTIR images from tumors perfused with PFA and $BaSO_4$-NP

Spectral Interval (cm^{-1})	Solid tumors (PFA)		Diffuse tumors (PFA)	
	Tissues	Capillaries	Tissues	Capillaries
1,216–1,158	0.0±0.0[a]	1.9±0.5[a,c]	0.0±0.0	0.0±0.0[c]
1,148–1,101	0.0±0.0[a]	0.5±0.3[a,c]	0.0±0.0	0.0±0.0[c]
1,101–1,038	1.2±0.07[a]	2.9±1.2[a]	1.4±0.2[b]	2.2±0.5[b]
1,101–1,034	1.4±1.2[a]	3.8±1.5[a]	1.7±0.2[b]	2.6±0.6[b]
992–969	0.0±0.0[a]	0.37±0.36[a]	0.0±0.0	0.03±0.5
1,148–969	4.3±1.3[a]	19.4±3.8[a,c]	5.0±0.7[b]	7.6±1.5[b,c]

All values are mean±SE of spectral integration results obtained from different spectral intervals

[a] Tumor solid is significantly different from capillaries solid

[b] Tumor diffuse is significantly different from capillaries diffuse

[c] Capillaries solid are significantly different from capillaries diffuse. No significant difference was found between solid and diffuse tumor tissue. n =6 samples and 50 spectra per sample

covering the absorptions of amides. The absorption difference found with spectra covering the tissue compartments was sufficient to discriminate all capillaries without exception. This choice of small Au-NP was due to the possibility to open this animal preparation to multimodal imaging with X-ray microscopy applications, for tomography or fluorescence. Au-NP have been recently proposed as high X-ray attenuation contrast agents for X-ray tomography [18] and were found useful for both high-resolution (50 nm spatial resolution) ex vivo imaging or low-resolution (1 μm) in vivo imaging for investigations on small animals (rodents). Our study on tissue sections using Au-NP to reveal tumor vasculature thus opens the way for a multimodal imaging of tumor blood vasculature using both X-ray tomography for morphological analyses and FTIR imaging for molecular histology. We also used $BaSO_4$ as high IR absorbing NP for enhancing the contrast between capillaries and tissue by FTIR imaging. As expected, we get much better results than by using Au-NP. The most important aspect of this study is that $BaSO_4$-NP can be used as biocompatible contrast agents for other multimodal imaging applications, combining μMRI [19], CT [20], or μPET imaging [21]. Therefore, again, our study opens the opportunity to couple 3D in vivo imaging techniques with FTIR imaging used as histology pathology tool. The advantage of FTIR imaging is to give ex vivo microscopic details on tumor blood vasculature [22, 23] that in vivo techniques cannot resolve (mm to sub-mm spatial resolutions only).

The second aim of our study was to demonstrate that the utilization of NP used for filling the blood vasculature of tumors could provide some information about fenestration of capillaries. We assumed that fenestration occurred because of the large number of cases found with tumor capillaries exhibiting extravascular diffusion of NP (n=30) with respect to normal tissue vessels (n=0). However, we must also consider that other phenomena than fenestration could participate to these observations, such as vascular membrane tearing or its incomplete formation during vessel sprouting in tumors [24]. Only a few reports have clearly shown fenestraes in brain tumor capillaries using electron microscopy [2, 25, 26], with dimensions ranging usually between 10 and 60 nm, but possibly up to 300 nm [2].

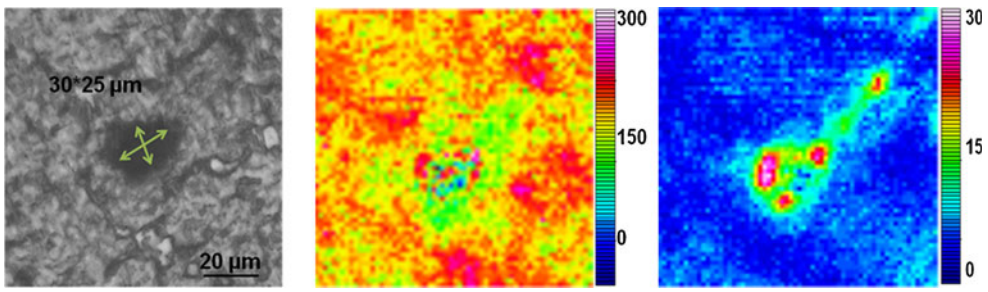

Fig. 4 FTIR imaging of solid tumor perfused with PFA and Au-NP. *Left*—mice brain tumor tissue section (20-μm thick) with a large coopted blood vessel. *Center*—2D-FTIR image of blood vessel (4,000–900 cm^{-1} spectral interval). *Right*—2D-FTIR image with highest absorption contrast for Au-NP vs. tissue using the 1,150–950 cm^{-1} spectral interval

Nevertheless, the objective was to reveal both the distribution of fenestraes (or vascular discontinuities [25]) and the extravascular diffusion space they offer using the two NP. The utilization of large NP ($BaSO_4$; ∅ 500 nm) as contrast agent was found to reveal extravascular diffusion of NP in only nine capillaries (8% of total tumor capillaries analyzed), with three specimen from solid tumor model and 6 from diffuse tumor model. A larger number of capillaries (21; 18% of total) and an inverse proportion between solid and diffuse tumor models (14 for solid and seven for diffuse models, respectively) were found to allow extravascular diffusion with the utilization of small NP (Au; ∅ 25 nm). One first important result is to find that only 8% to 18% of capillaries tested on 20-μm-thick tissue sections could reveal extravascular diffusion. This small proportion seems coherent with the physiological notion of limited vascular membrane fenestration to maintain intravascular fluid pressure for blood flow dynamics. The second major result is the proportion of small and large vascular fenestrations found in solid and diffuse tumors, which was found inversed: smaller but more numerous in solid tumors and thus larger but in more limited number in diffuse tumors. The results obtained on the solid tumor model are compliant with the notion that solid tumors are more angiogenic, thus they produce a huge number of small capillaries (true neoangiogenesis) which can be fenestrated, thus leading to a larger number of small fenestraes [6]. On the other hand, cells of diffuse tumors models are more coopting existing blood vessels to modify their structure and vascular membrane for higher diffusion, notably in the brain where the BBB normally prohibits free vascular trafficking. It has been reported that diffuse gliomas may exhibit quite large fenestraes on coopted vessels [27]. One important result was to find no healthy tissue blood capillary exhibiting extravascular diffusion of NP, whatever we considered Au-NP of $BaSO_4$-NP, thus confirming that vascular discontinuities where present only in tumor vasculatures. Finally, if we cannot conclude about the existence of fenestraes in our solid and diffuse tumor models, it appeared that FTIR imaging could at least reveal vascular discontinuities, which were found in larger number but with smaller dimensions in solid tumors, while the diffuse tumor model exhibited fewer specimens but with larger dimensions.

Conclusion

This FTIR imaging study has shown that nanoparticles used as imaging contrast agents can be used for revealing both the density of capillaries in tumor tissues and the extravascular diffusion space vascular discontinuities offer to peripheral tumor cells. The approach was selective enough to discriminate between vasculatures of healthy and solid and diffuse models of glioma tumors. We can thus suggest pushing the development of FTIR imaging as a functional histology tool for fundamental and applied investigations on tumor vasculature.

Acknowledgments The author is indebted to the contribution of "Association Française contre les Myopathies" (AFM—contract no. 14258), the "Ligue Nationale contre le cancer," and the "Agence Nationale de la Recherche" (ANR—contract no. bl-inter09_464249—MIAG-X) for their financial supports. This research was also partially supported within the EU 7th Framework Programme (FP7/2007–2013) under the grant agreement no. 226716.

References

1. Jain RK, Munn LL (2000) Nat Med 6:131–132
2. Roberts WG, Palade GE (1997) Cancer Res 57:765–772
3. Roberts WG, Palade GE (1995) J Cell Sci 108(Pt 6):2369–2379
4. Vaupel P (2004) Semin Radiat Oncol 14:198–206
5. Hobbs SK, Monsky WL, Yuan F, Roberts WG, Griffith L, Torchilin VP, Jain RK (1998) Proc Natl Acad Sci USA 95:4607–4612
6. Shibata S (1989) Acta Neuropathol 78:561–571
7. Engelhorn T, Eyupoglu IY, Schwarz MA, Karolczak M, Bruenner H, Struffert T, Kalender W, Doerfler A (2009) Neurosci Lett 458:28–31
8. Gambarota G, Leenders W, Maass C, Wesseling P, van der Kogel B, van Tellingen O, Heerschap A (2008) Br J Cancer 98:1784–1789
9. Lüdemann L, Grieger W, Wurm R, Wust P, Zimmer C (2005) Magn Reson Imaging 23:833–841
10. Petibois C, Déléris G (2006) Trends Biotechnol 24:455–462
11. Bernsen HJ, Rijken PF, Hagemeier NE, van der Kogel AJ (1999) Microvasc Res 57:244–257
12. Fernandez DC, Bhargava R, Hewitt SM, Levin IW (2005) Nat Biotechnol 23:469–474
13. Petibois C, Drogat B, Bikfalvi A, Deleris G, Moenner M (2007) FEBS Let 581:5469–5474
14. Miller FA, Wilkins CH (1952) Anal Chem 24:1253–1294
15. Amirouche-Korichi A, Mouzali M, Watts DC (2009) Dent Mater 25:1411–1418
16. Liu C-J, Wang C-H, Chien CC, Yang T-Y, Chen S-T, Leng WH, Lee C-F, Lee K-O, Hwu Y, Lee Y-C, Cheng C-L, Yang C-S, Chen YJ, Je JH, Margaritondo G (2008) Nanotechnology 19:1–6
17. Usha R, Ramasami T (2000) Thermochim Acta 356:59–66
18. Chien CC, Wang CH, Wang CL, Li ER, Lee KH, Hwu Y, Lin CY, Chang SJ, Yang CS, Petibois C, Margaritondo G (2010) Anal Bioanal Chem 397:2109–2116
19. Rasmussen AS, Lauridsen H, Laustsen C, Jensen BG, Pedersen SF, Uhrenholt L, Boel LW, Uldbjerg N, Wang T, Pedersen M (2010) BMC Physiol 10:3
20. Oses P, Renault MA, Chauvel R, Leroux L, Allieres C, Seguy B, Lamaziere JM, Dufourcq P, Couffinhal T, Duplaa C (2009) Arterioscler Thromb Vasc Biol 29:2090–2092
21. Leng H, Wang X, Ross RD, Niebur GL, Roeder RK (2008) J Mech Behav Biomed Mater 1:68–75
22. Petibois C, Desbat B (2010) Trends Biotechnol 28:495–500
23. Wehbe K, Pinneau R, Moenner M, Deleris G, Petibois C (2008) Anal Bioanal Chem 392:129–135
24. Kim JH, Park JA, Lee SW, Kim WJ, Yu YS, Kim KW (2006) J Biochem Mol Biol 39:339–345
25. Molnar PP, O'Neill BP, Scheithauer BW, Groothuis DR (1999) Neuro Oncol 1:89–100
26. Ribatti D, Nico B, Morbidelli L, Donnini S, Ziche M, Vacca A, Roncali L, Presta M (2001) J Vasc Res 38:389–397
27. Kawasaki K, Kohno M, Inenaga C, Sato A, Hondo H, Miwa A, Fujii Y, Takahashi H (2009) Neuropathology 29:85–90